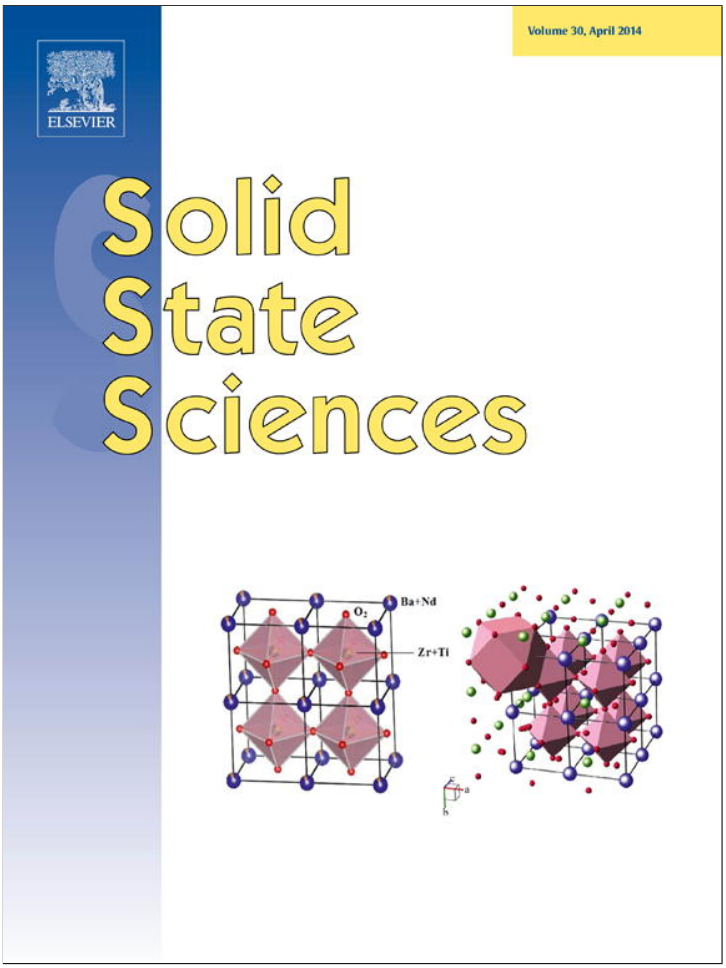

Solid State Sciences 30 (2014) 94–104

Contents lists available at ScienceDirect

Solid State Sciences

journal homepage: www.elsevier.com/locate/ssscie

The route to $MB_xN_yC_z$ molecular wheels: II. Results using accurate functionals and basis sets

A. Güthler [a], S. Mukhopadhyay [b], R. Pandey [b], I. Boustani [a,*]

[a] Bergische Universität Wuppertal, FB C – Mathematik und Naturwissenschaften, Gaußstraße 20, 42119 Wuppertal, Germany
[b] Michigan Technological University, Department of Physics, Houghton, MI 49931, USA

ARTICLE INFO

Article history:
Received 25 February 2013
Received in revised form
8 October 2013
Accepted 23 October 2013
Available online 7 November 2013

Keywords:
Molecular wheels
TiBn clusters
Ab initio calculations

ABSTRACT

Applying *ab initio* quantum chemical methods, molecular wheels composed of metal and light atoms were investigated. High quality basis sets 6-31G*, TZPV, and cc-pVTZ as well as exchange and non-local correlation functionals B3LYP, BP86 and B3P86 were used. The ground-state energy and structures of cyclic planar and pyramidal clusters TiB_n (for $n = 3–10$) were computed. In addition, the relative stability and electronic structures of molecular wheels $TiB_xN_yC_z$ (for $x, y, z = 0–10$) and MB_nC_{10-n} (for $n = 2$ to 5 and M = Sc to Zn) were determined. This paper sustains a follow-up study to the previous one of Boustani and Pandey [Solid State Sci. 14 (2012) 1591], in which the calculations were carried out at the HF-SCF/STO3G/6-31G level of theory to determine the initial stability and properties. The results show that there is a competition between the 2D planar and the 3D pyramidal TiB_n clusters (for $n = 3–8$). Different isomers of TiB_{10} clusters were also studied and a structural transition of 3D-isomer into 2D-wheel is presented. Substitution boron in TiB_{10} by carbon or/and nitrogen atoms enhances the stability and leads toward the most stable wheel TiB_3C_7. Furthermore, the computations show that Sc, Ti and V at the center of the molecular wheels are energetically favored over other transition metal atoms of the first row.

1. Introduction

The physics and chemistry of boron were always very interesting and exciting fields due to the particular and anomalous bonding features of boron recorded theoretically and experimentally. From the well known boron hydrides with its marvelous forms, over benzene-like structures of borazines, up to polyhedral structures of pure boron, or new boron solids, it is a true challenge to discover novel boron structures [1,2]. The development of non-crystalline boron beyond the tetragonal, octahedral or icosahedral arrangements began at the end of the eighties as Hanley and Anderson [3,4] attempted to find magic numbers in the mass-spectra of small boron clusters. Different theoretical studies were carried out to interpret the experimental features [5–7]. In the nineties and the following years novel quasiplanar boron clusters [8,9], boron nanotubes [10–12], boron fullerenes and sheets [13–15] were theoretically proposed and predicted.

Our first attempt to investigate elemental boron clusters was in 1990 [16], published in part by Bonaĉić-Koutecký et al. [17], completed in 1994 by Boustani [18]. In the former one we used the self-consistent-field (SCF) of the Hartree–Fock (HF) as well as the configuration interaction (CI) theory to determine the geometrical and electronic structures of singly and doubly ionized boron clusters B_n for ($n = 2–8$). The most important results were that the optimized neutral and charged boron clusters possess planar structures except of B_7, which has a quasi-planar geometry in form of distorted hexagonal pyramid, whose apical atom lies slightly above the plane. Furthermore, the structure of $B_8–D_{7h}$ ($^3A_2'$) was also planar and composed of a heptagon with a central atom and presents the first boron molecular wheel.

Wang, Boldyrev and co-workers [19] were very active theoretically and experimentally. They were able to detect and confirm hepta- and octa-coordinate boron in molecular wheels of eight- and nine-atom boron clusters. All investigated B_8, B_8^-, B_8^{2-}, B_9 and B_9^- clusters have planar wheel structure. They found that the double aromatic character in chemical bonding was responsible for their planarity and thus confirming the wheel geometry of the B_8 cluster which was predicted by Boustani et al. [16] and mentioned by Bonaĉić-Koutecký et al. [17]. The radii in these clusters were between 1.8 and 2.0 Å. The concept of double aromaticity in unusual bonding was already proposed by Schleyer and co-workers [20]. That means σ and π bonding are highly delocalized and responsible

* Corresponding author. Tel.: +49 202596665.
E-mail address: boustani@uni-wuppertal.de (I. Boustani).

1293-2558/$ – see front matter © 2013 Elsevier Masson SAS. All rights reserved.
http://dx.doi.org/10.1016/j.solidstatesciences.2013.10.010

for the planarity and aromaticity of the B_8^{2-}, and B_9^- clusters. Additional study of the latter anionic boron clusters was carried out by Fowler and Gray [21] showing ring current characteristic of aromatic systems. They concluded that their stability refers to the double ($\sigma + \pi$) aromaticity and also obeys the Hückel ($4n + 2$) electron counting rule. Furthermore, Tai et al. [22] predicted that B_{20}^{2-} cluster exhibits a planar sheet-like structure but its MO picture does not follow the Hückel rule ($4n + 2$). They proposed the concept of *disk aromaticity*, which discriminates between π-bands and σ-bands. The in-plane bonding is to be attributed to 25 occupied σ-orbitals, while the out-of-plane bonding is to be attributed to six occupied π-orbitals. They found that B_{20}^{2-} cluster exhibits remarkable inner paratropic current in the σ-channel and an outer diatropic current in the π-channel.

Due to the familiar nuclear magnetic resonance (NMR) chemical shift convention, Schleyer and co-workers [23] proposed a new aromaticity/antiaromaticity criterion. They considered the signs of the computed values to be reversed: Negative *nucleus-independent chemical shifts* (NICS) values denote aromaticity; positive NICS values, at the other hand, stands for antiaromaticity. In order to verify this issue, they calculated NICS values for individual rings in polycyclic systems at the GIAO-SCF/6-31+G* level of theory. For example, the negative values NICS for benzene = −9.7 and for naphthalene = −9.9, indicate their aromaticity, while the positive NICS value of the four-membered ring in benzocyclobutadiene = +22.5, shows its antiaromaticity. Further support for the argument of double aromaticity and planarity of boron clusters was done by Boldyrev, Wang and co-workers [19], calculating the NICSs of B_8^{2-} and B_9^- clusters at the B3LYP/6-311++G** level. The rather high NICS[1] of these clusters in the range of 0.5–3.0 Å above the center, were −3.7 to −27.0 and −3.8 to −23.2 for B_8^{2-} and B_9^-, respectively. Due to the delocalized bonding however, they pointed out that individual bonding between the central boron and the surrounding boron atoms cannot exist. Instead they suggested the term *disk delocalization* to describe the bonding features in these clusters.

Similarly, Wang and Boldyrev groups theoretically investigated metal boron rings by means of more sophisticated methods of theory and photoelectron spectroscopy (PES) [24]. They experimentally detected the aromatic metal centered monocyclic boron rings CoB_8^- (D_{8h}, $^1A_{1g}$) and RuB_9^- (D_{9h}, $^1A_1$). The shape of the anionic and neutral clusters are planar with a slight distortion. The Ru atom is only 0.1 Å out-of-plane. The distances from the metal center to the boron and between the peripheral boron atoms for the CoB_8^- cluster were found to be 2.033 and 1.556 Å, respectively. For the CoB_8 (D_{2h}, $^1B_{2u}$) cluster, different distances varying from 2.069 to 2.010 Å and 1,572, 1.545 Å were calculated.

Wei-Li Li et al. [25] investigated the interplay between electronic and geometric requirements also for the wheel system anion VB_{10}^-. According to their findings, 3d transition metals fit both of these requirements to build eight- and nine-membered boron ring wheels, but are too small to suffice the geometrical needs. It is therefore natural to ask, what the maximum coordination number in a planar (carbon and boron) cluster is. Heine and Merino [26] concluded that despite the electron-deficient feature and the fact that deltahedral bonding predominate in boron compounds, $M@B_9^-$ (M = Ru, Rh, Ir) clusters can form strong localized 2c–2e (two centered-two electron) σ-bonding between the ring atoms and σ in-plane and π out-of-plane delocalized bonding. In the later case, by satisfying the Hückel-rule $4N + 2$, the central metal atoms participate to the σ delocalized bonding. Thus the participation of metal atoms in σ bonds is essential to stabilize these structures. Therefore, the reason for the stability stems mainly from the double-aromaticity of σ and π bonds [20].

Boldyrev group uses the MO-Theory and the phenomenon of double aromaticity to explain the unusual bonding in boron wheels, Boustani [18] originally uses the concept of sp^2-hybridization to describe bonding in pure planar boron clusters. The main reason for the stability of planar boron clusters stems from the resonance energy. In this context, Gutman et al. [27] and Aihara [28] proposed and used theoretically more sophisticated methods such as graph-theoretical-approach to calculate the so-called *Topological Resonance Energy* (TRE). Aihara and co-workers [29] noted that the widely used Hückel $4N + 2$ rule is restricted to monocyclic systems only. An application of the hybridization approach and the quantitative methods of the TRE to monocyclic $M@B_n$ wheel-system is not yet accomplished.

Boron wheels and related energy minima were studied by Liao et al. [30]. They claimed that there is a phenomenon, which makes the search for energy minima in these clusters a very complex task. Many of the boron wheels, mentioned so far, exhibit local but no global minima. They also showed that global minima of doped (neutral) boron wheels $M@B_n$ (M is a main group element) are missing. Only the triplet $Be@B_8$ wheel has a global minimum.

Wang, Boldyrev and co-workers continued working on molecular wheels and succeeded in predicting and detecting planar metallic boron clusters with the so far highest coordination number $M@B_{10}^-$ (M = Nb, Ta) [31]. They presented the so-called *Adaptive Natural Density Partitioning* (AdNDP) analysis which has the ability to simultaneously recover both localized and delocalized bonding in chemical species. The AdNDP analysis revealed ten 2c–2e peripheral σ bonds, five delocalized σ bonds (satisfying the $4N + 2$ rule for aromaticity with $N = 2$), and three delocalized π bonds (satisfying the $4N + 2$ rule for aromaticity with $N = 1$). A similar bonding pattern was found for $Nb@B_{10}^-$. Thus, both clusters are doubly σ and π aromatic and satisfy their construction model. They also found that in contrast to the molecular wheels of B_8^{2-}, B_9^-, and $Ru@B_9^-$, there are 10 delocalized σ electrons for the current $M@B_{10}^-$ molecular wheels owing to the strong bonding between the 4d/5d orbitals of Nb/Ta with the peripheral B_{10}^- ring.

Furthermore, Wang et al. [32] investigated small titanium carbide clusters TiC_x^- (for $x = 2–5$) using magnetic-bottle time-of-flight photoelectron spectroscopy. They obtained vibrationally resolved photoelectron spectra and rich low-lying electronic excited states for a series of TiC_x clusters. They observed that electron affinities and the ground-state vibrational frequencies are tentatively interpreted to support planar ring-type structures of these clusters.

The most recent paper about molecular wheels $M@B_n$ (for $n \leq 10$) was published by Boustani and Pandey [33]. They reported the electronic and geometrical structures of transition metal atoms surrounded by boron atoms, calculated at the HF-SCF/STO3G and HF-SCF/6-31G level of theory. They investigated the change in stability when boron is replaced by nitrogen and carbon atoms. They also studied the $MB_xN_yC_z$ system, where M is the transition metal atoms varying from Sc to Zn, while x, y and z are the number of B, C and N atoms in the clusters. They found that all 2D-structures were more stable than the 3D-ones. The HF-SCF calculations have shown that the planar TiB_n fan-like structures (for $n = 3–8$) are the most stable isomers, and the binding energy E_b is varying between 2.47 and 3.41 eV/atom. They also studied doped clusters such as TiB_nN_{10-n}, TiB_nC_{10-n} and TiC_nB_{10-n}. They asserted that the E_b of TiB_n increases with increasing n up to a value of $E_b = 3.69$ eV/atom for $n = 10$. After doping with nitrogen the E_b of TiB_nN_{10-n} increases to a maximum of 5.0 eV/atom by $n = 5$ resulting the TiB_5N_5 isomer. Further doping with carbon atoms in the TiB_nC_{10-n} system improves the E_b values and leads to a maximum at 6.25 eV/

[1] All measured in ppm.

atom by $n = 5$ having TiC_5B_5 as the most stable molecular wheel at the HF-SCF/6-31G level of theory.

In order to understand the influence of the central atom of the wheels on the stability E_b and the nature of the involved bonds, Boustani and Pandey [33] replaced the central atom by transition metal atoms of the first row. They studied again the MC_5B_5[2] molecular wheels for M = Sc to Zn and found that those with central elements Sc, Ti and Fe have higher binding energy than others. The calculations of wheels with the Sc, Ti and Fe atoms at the center, considered at the 6-31G/B3LYP level of theory, show that the Sc-centered wheel is about 0.03 eV more stable than the Ti-, and Fe-centered wheels.

Finally, the current paper is a follow up study of Boustani and Pandey [33], as described in the previous sections. It sustains the investigation of metal boron clusters and molecular wheels beyond the HF-SCF method towards higher level of theory and accurate basis sets, as already mentioned above. This paper is organized as follows: Section 2 describes the Computational methods, Section 3 presents the Results and discussion, and Section 4 closes the paper with Summary and conclusions.

2. Computational methods

Ab initio quantum chemical methods for solving the many-electron problems in the framework of the Hartree–Fock self-consistent-field (HF-SCF) as well as the Kohn–Sham equations within the density functional theory (DFT) were applied to determine the ground state energies of the molecular systems. The computations of the current follow-up study of the previous paper [33] are carried out at higher level and accuracy of functionals and basis sets beyond the HF-SCF level of theory. The exchange-correlation functionals are estimated by the generalized gradient approximation (GGA) using BP86, as hybrid functionals of exchange of Becke [34] and non-local correlation of Perdew [35], then B3P86 as a hybrid functionals of three-parameter exchange of Becke [36] and non-local correlation of Perdew [35]. In addition we used B3LYP, the three-parameter hybrid exchange functional of Becke [36], and the non-local correlation functional of Lee, Yang and Parr [37].

Besides the exchange-correlation functionals, all-electron calculations in the current work were performed using high quality basis sets namely the split valence (6-31G*) with appended polarization functions and the triple-zeta (TZVP) including *d*-functions on metal atoms and p-functions on boron and carbon. In addition to that, a much higher quality correlation-consistent polarized valence-only triple zeta (cc-pVTZ) basis set was used to determine the relative stability, energies, electronic states and properties of the systems. The optimization procedure, based on the analytical gradient method and determined for the high quality basis sets and exchange-correlation functionals, has been carried out to locate a minimum on the potential energy hypersurface and to predict equilibrium structures of the molecular systems. After the optimization process it is necessary to determine the binding energy per atom of the metal clusters and molecular wheels as a measure for their stability. The binding energy per atom (E_b) in eV/atom is defined as follows:

$$E_b = \frac{1}{n}\{E(M) + xE(B) + yE(C) + zE(N) - E(MB_xC_yN_z)\} \quad (1)$$

where n is the total number of atoms in the clusters, $E(M)$ is the energy of transition metal atoms M = Sc, Ti, V, Cr, Mn, Fe, Co, Ni, Cu and Zn, where $E(B)$, $E(C)$, and $E(N)$ are the energies of boron, carbon, and nitrogen atoms, respectively. $E(MB_xC_yN_z)$ is the energy of the cluster or of the molecular wheel, while x, y and z are the number of compounds in the cluster or wheel. Symmetry constraints were considered in the form of a point group symmetry. In all calculations, the spin-polarized DFT calculations were carried out for different spin states of each individual atom, cluster and wheel, selecting the lowest spin state energy to be the ground state energy. These calculations were carried out using the following program packages: Gamess_UK [38], NWChem [39], ORCA [40], and Gaussian 03 [41].

3. Results and discussion

After considering higher level of theory, in which exchange-correlation functionals as well as high quality basis sets are deployed, the general sequence of reported results in Ref. [33] is confirmed but with some exceptions. In this section we present the 2D TiB_n (for $n = 3–10$) clusters in comparison with the 3D systems announced in our previous paper [33]. Then we depict some 3D TiB_{10} isomers and illustrate the transition of one 3D TiB_{10} structure into a planar TiB_{10} molecular wheel. Afterward we present the stability of $TiB_xC_yN_z$ systems as function of x, y and z, each is varying between 1 and 10. Then we discuss the $TiB_nN_mC_{10-n-m}$ systems (for $n = 2$ and 3, $m = 1$ and 2) and finally the MC_nB_{10-n} systems (for M = Sc to Zn and $n = 5–8$).

3.1. Competition between the 2D and 3D TiB_n systems

The current calculations of the TiB_n systems (for $n = 1–10$), carried out at the BP86/6-31G* level of theory, include two kinds of planar and one kind of pyramidal structures. The first kind of planar structures are those fan-like clusters, in which only one atomic distance between the Ti atom and the boron atoms is considered as a variable. That means the boron atoms have the same bondlength to the Ti atoms in the fan-like structures. These 2D clusters are assigned as TiB_n (fixed) (for $n = 1–10$) and presented in our previous paper [33]. The second kind of planar structures are those fan-like clusters, in which all atomic distances between the Ti atom and the boron atoms are considered as variables. These clusters are assigned as TiB_n (Opt) (for $n = 1–10$) and presented in (Fig. 1) in this paper. After the optimization procedure these structures show that the Ti atom is connected only to two boron atoms. The third kind of structures are those of pyramidal form in which the apex atom is always Ti. These pyramidal TiB_n structures (for $n = 3–8$) are presented in (Fig. 3). The 3D non-pyramidal TiB_9 and TiB_{10} structures of umbrella-like character, discussed in Ref. [33], are also calculated and the latter structure is presented in (Fig. 4) and assigned by C_{9v}. The E_b of the three kinds of structures are listed in Table 1.

The values of the binding energy E_b of the optimized planar fan-like TiB_n (fixed) structures (for $n = 1–10$), obtained at the HF-SCF/STO3G level, are improved remarkably at the BP86/6-31G* level of theory. The following comparison between the E_b values obtained at the HF-SCF/STO3G in Ref. [33] and BP86/6-31G* levels (this work) shows the improvements in details. Only for the dimer TiB, the related E_b value reduces from 1.83 to 1.40 eV/atom, while the E_b of the triangular trimer TiB_2 increases from 2.32 to 2.58 eV/atom, and of TiB_3 also increases from 2.47 to 3.18 eV/atom. Similarly the E_b of TiB_4 rises from 2.88 to 3.54 eV/atom, while that of TiB_5 enhances by 0.66 eV/atom. The E_b of the TiB_6 climbs up from 3.17 to 4.01 eV/atom, while by TiB_7 it increases from 3.29 to 4.14 eV/atom. The E_b of TiB_8 raises from 3.41 to 4.22 eV/atom and by TiB_9 from 3.42 to 4.41 eV/atom. Finally the E_b of TiB_{10} increases from 3.69 to 4.85 eV/atom. Only the values of TiB_n(Fixed), obtained at the BP86/6-31G* level and reported in Table 1, are presented in (Fig. 6) as a function of the number of boron atoms. This function is the lowest one in (Fig. 6) assigned by black circles.

[2] All MC_5B_5 clusters exhibit the D_{5h}-point group symmetry.

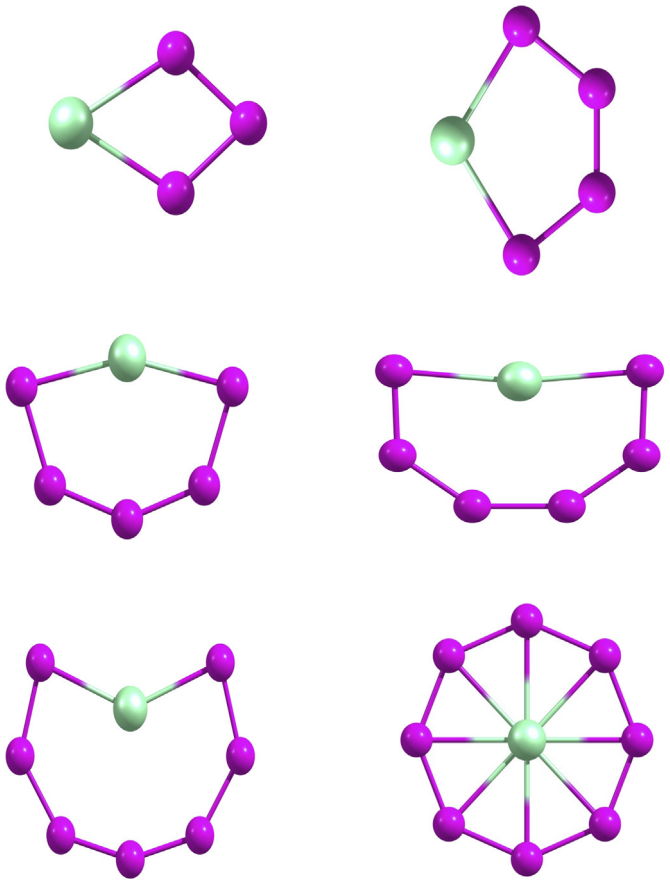

Fig. 1. The fan-like 2D TiB_n clusters for (n = 3–7) and TiB_8 wheel.

The calculations in our previous paper [33] showed that the 2D TiB_n clusters (for n = 4–8) at the HF-SCF level are energetically favored over the 3D TiB_n ones. Contrastingly, the present calculations at the BP86/6-31G* level of theory show that the 2D and 3D TiB_n clusters (for n = 3–8) are energetically in competition. Only the 2D TiB_n clusters (for n = 9 and 10) as wheels are still the favored structures. In both types of clusters, the 2D fan-like and 3D pyramidal structures, the Ti atom remains as an apex atom.

At the current BP86/6-31G* level of theory, the Ti atoms in the planar fan-like structures of the 2D TiB_n(Opt) clusters (for n = 3–7) lose some bonds to boron atoms after structural reoptimization. The optimized structures indicate that the Ti atom is connected to only two boron atoms keeping its position mostly at the focus of an arc formed by boron atoms, as can be seen in (Fig. 1). By inspection of the total electron charge density of TiB_5 and TiB_7, as representative for planar fan-like clusters, one can see that the electron density expands along the arc of boron atoms oppositely to the Ti atom (Fig. 2). By the pyramidal 3D TiB_n clusters, the apex Ti atom is always connected to all boron atoms at the basis and the heights of the pyramids decrease with increasing the number of boron atoms,

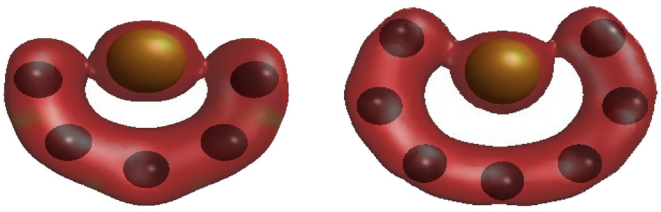

Fig. 2. The total electron density of the 2D TiB_5 (left) and TiB_7 (right) clusters.

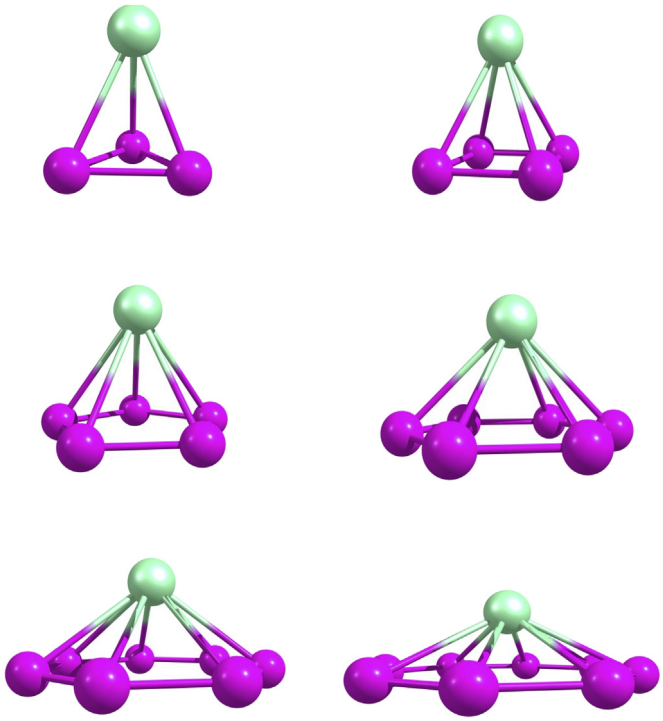

Fig. 3. The pyramidal 3D TiB_n clusters for (n = 3–8).

as can be seen in (Fig. 3). In other words: by increasing the number of boron atoms, the pyramids flat simply out towards wheels. The binding energy per atom of the 2D and 3D TiB_n systems for (for n = 2–10) are listed in Table 1.

The calculated ground state of the dimer TiB is $C_{\infty v}$ ($^2\Sigma^+$) with an atomic distance of 2.03 Å. The binding energy reduces from 1.83 eV/atom at the HF-SCF/STO3G to 1.4 eV/atom at BP86/6-31G* level. The ground state of the equilateral triangle TiB_2 with Ti as an apex atom is C_{2v} ($^3A_2$). Both bondlength of Ti–B and B–B are 2.05 and 1.55 Å, respectively. The corresponding E_b increases to 2.85 eV/atom after structural optimization. The ground state of the planar TiB_3 cluster is C_{2v} ($^2A_2$). The bondlength between Ti atom and two outer boron atoms is 2.0 Å, while the atomic distance between the boron atoms is 1.55 Å. The E_b of the 2D TiB_3 cluster is 3.57 eV/atom. This value is slightly larger than the corresponding one of the trigonal pyramid TiB_3 of 3.42 eV/atom. The ground state of the trigonal pyramid is C_{3v} ($^4A_1$) and the bondlength of the Ti atom to the three boron atoms in the basis is 2.1 Å, while the bondlength between the boron atoms is 1.63 Å. The height of the trigonal pyramid is 1.87 Å.

The binding energy 3.86 eV/atom of the tetragonal pyramidal TiB_4 cluster is slightly larger than the planar fan-like TiB_4 cluster of 3.80 eV/atom. The ground states of the 3D and 2D TiB_4 clusters are C_{4v} ($^3A_1$) and C_{2v} ($^3B_1$), respectively. The bondlength of the Ti apex atom to the basis of four boron atoms is about 2.1 Å. The bondlength of the boron square is 1.63 Å and the height of the pyramid is about 1.73 Å. By the planar structure the Ti atom is connected to only two boron atoms with a bondlength of 2.05 Å, while the bondlength between the two boron atoms opposite to Ti is 1.55 Å. The other counterpart distances are 1.56 Å. The ground state of planar fan-like structure TiB_5 is C_{2v} ($^2B_2$) and the corresponding bondlength of Ti–B and twice B–B are 2.06, 1.55 and 1.54 Å, respectively. The binding energy E_b 4.07 eV/atom of the 2D TiB_5 cluster is very close to the corresponding one of the pentagonal pyramidal TiB_5 cluster of 4.05 eV/atom. The ground state of the 3D TiB_5 cluster is C_{5v} ($^2A_1$) and the bondlength between the apex atom Ti and the basis of five

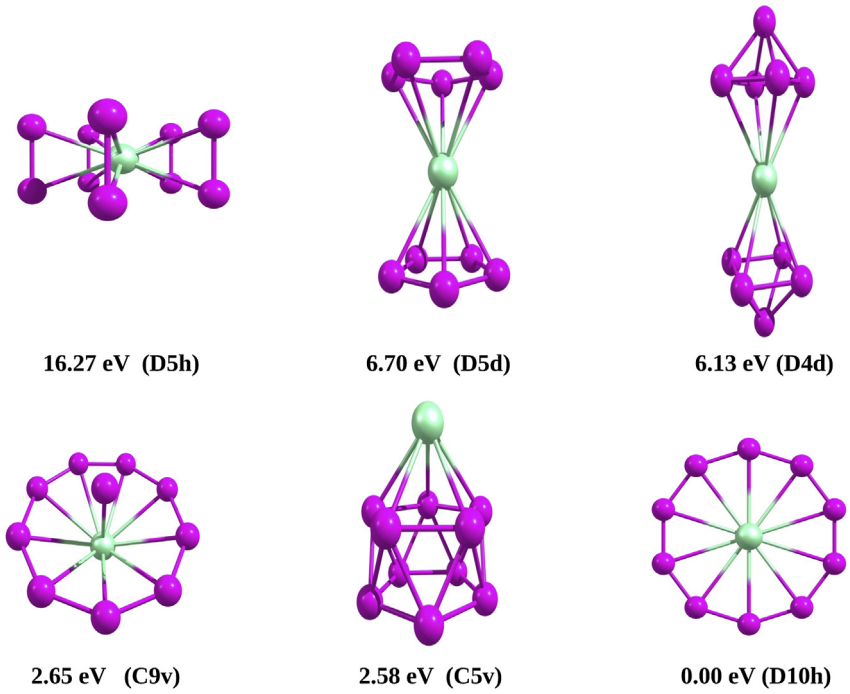

Fig. 4. The TiB_{10} isomers indicated by the relative energies to the wheel and assigned by the point group symmetry.

boron atoms is 2.24 Å. The bondlength of the pentagon is 1.6 Å and the height of the pentagonal pyramid is 1.78 Å.

The hexagonal pyramidal TiB_6 cluster is by 0.10 eV/atom more stable than the planar TiB_6 one. The ground states of both structures are C_{6v} ($^3A_1$) and C_{2v} ($^2B_2$), respectively. The bondlength between the apex atom Ti and the basis of the six boron atoms of the hexagonal pyramid is 2.2 Å, while the bondlength of the hexagon is 1.59 Å and its height is 1.52 Å. The Ti atom of fan-like 2D TiB_6 cluster is linked to only two boron atoms with 2.06 Å. The bondlengths of the following boron atoms of the arc are 1.57, 1.56 and 1.55 Å. The ground states of the heptagonal pyramid and planar fan-like TiB_7 clusters are $C_{7v}(^2A)$ and $C_{2v}(^2B_2)$,, respectively. The calculated E_b of the 3D TiB_7 is 4.50 eV/atom, while that of the 2D TiB_7 is about 4.27 eV/atom. This means that the heptagonal pyramid TiB_7 is with 0.23 eV/atom more stable than the planar fan-like TiB_7. The bondlength between the Ti atom and the two boron atoms is 2.08 Å and the average atomic distance between the boron atoms of the arc is 1.56 Å. On the other hand, the atomic distance between the apex atom Ti and the boron atoms at the basis of the heptagonal pyramid is 2.25 Å, while the bondlength of the heptagon is 1.58 and its height is 1.33 Å.

The harmonic vibrational frequencies (HVF) of the 2D and 3D TiB_n boron clusters for ($n = 3$–7) are calculated. Both HVF values for 2D and 3D Ti_3 clusters are positive with 170–1146 cm^{-1} and 162 to 3878 cm^{-1}, respectively. One of the HVF values for the 2D Ti_4 cluster is negative, while those of the 3D Ti_4 cluster are positive with 241–889 cm^{-1}. The positive HVF values for 2D Ti_5 cluster are 151–2457 cm^{-1}, while four of the HVF values of 3D Ti_5 cluster are negative. The HVF values for the 2D Ti_6 cluster are 69–1501 cm^{-1}, while for the 3D Ti_6 cluster only value of the HVF is negative. Finally tow HVF values for the 2D and 3D Ti_7 cluster are negative. This means that clusters with negative frequencies have simply transition structures.

The planar octagonal wheel and the octagonal pyramid TiB_8 have similar geometries and energies, however differ slightly in the positions of the central Ti atom. The ground states of both structures are D_{8h} ($^5B_{1g}$) and C_{8v} ($^5A_1$). The corresponding E_b of 2D and 3D clusters are around 4.62 and 4.69 eV/atom, respectively. The atomic distance between the central atom Ti and the octagon in the 2D TiB_8 cluster is 2.13 Å, while the bondlength of the octagon is 1.62 Å. Both distances in the octagonal pyramid decrease to 2.07 Å for Ti–B, and to 1.59 Å for B–B, while its height lowers only to 0.8 Å.

The molecular wheels TiB_9 and TiB_{10} of D_{9h} and D_{10h} symmetry, calculated at the BP86/6-31G* level in the C_s symmetry and corresponding ground states $^2A'$ and $^3A'$, are still with 0.03 and 0.25 eV/atom more stable than the 3D TiB_9 and TiB_{10} umbrella-like or satellite dish-like clusters. The radii in the 2D wheels as atomic distance between the central atom Ti and the boron atom wheels of TiB_9 and TiB_{10} clusters are 2.34 and 2.49 Å, while the B–B distances in the nonagon and decagon are 1.60 and 1.54 Å, respectively. The 3D umbrella-like TiB_9 cluster of C_{8v} calculated in C_s symmetry has the ground state $^2A'$. The atomic distance of the Ti atom to the boron atoms of the octagon is 2.52 Å, while the distance between Ti and boron atom located at the focus is 2.07 Å. The B–B distance in the octagon is 1.54 Å. The 3D umbrella-like TiB_{10} cluster of C_{9v}, calculated in C_s symmetry with the ground state $^2A'$, is shown in (Fig. 4). The atomic distance of the Ti atom to the boron atoms of the nonagon is 2.46 Å, and to the boron atom at the focus is 2.08 Å. The B–B distance in the nonagon is about 1.56 Å.

3.2. *The TiB_{10} isomers and the transition from 3D into 2D*

In order to ensure that the molecular wheel of the TiB_{10} cluster is the most stable structure of this system, we have investigated few 3D TiB_{10} isomers at the BP86/6-31G* level of theory. The structures of the TiB_{10} isomers were optimized in some symmetry constraints, as shown in (Fig. 4). Of course there are many other geometrical possibilities for 3D structures. However, the geometries presented in (Fig. 4) were adopted from common structures known in the (in) organic chemistry. We have also listed the relative energies to the most stable structure, the molecular wheel TiB_{10}. In addition, we have simulated the transition of the 3D into 2D structure in such a way that two pentagons localized above and below Ti atom, like the D_{5d} structure in (Fig. 4), are approaching to each other forming the

Table 1
Point-group symmetry, spin-multiplicity and ground-state, binding energies E_b (eV/atom) of 2D and 3D TiB_n clusters, determined at the BP86/6-31G*.

n	TiB_n	2D (Fixed)	E_b	2D (Opt.)	E_b	3D (Opt.)	E_b
10	TiB_{10}	$D_{2h}(^3B_{3g})$	4.85	$C_s(^3A')$	4.86	$C_s(^3A')$	4.61
9	TiB_9	$C_{2v}(^2B_2)$	4.41	$C_s(^2A')$	4.77	$C_s(^2A')$	4.74
8	TiB_8	$D_{2h}(^3B_{2u})$	4.22	$D_{8h}(^5B_{1g})$	4.62	$C_{8v}(^5A_1)$	4.69
7	TiB_7	$C_{2v}(^3B_2)$	4.14	$C_{2v}(^2B_2)$	4.27	$C_{7v}(^2A_1)$	4.50
6	TiB_6	$C_{2v}(^3B_2)$	4.01	$C_{2v}(^3B_2)$	4.17	$C_{6v}(^3A_2)$	4.27
5	TiB_5	$C_{2v}(^2B_2)$	3.83	$C_{2v}(^2B_2)$	4.07	$C_{5v}(^2A_2)$	4.05
4	TiB_4	$C_{2v}(^3B_2)$	3.54	$C_{2v}(^3B_1)$	3.80	$C_{4v}(^3A_1)$	3.86
3	TiB_3	$C_{2v}(^2B_2)$	3.18	$C_{2v}(^2A_2)$	3.57	$C_{3v}(^4A_1)$	3.42
2	TiB_2	$C_{2v}(^3B_2)$	2.58	$C_{2v}(^3A_2)$	2.85	–	–
1	TiB	$C_{\infty v}(^2\Sigma^+)$	1.40	$C_{\infty v}(^2\Sigma^+)$	1.40	–	–

wheel. These snapshots of the structural transformation are presented in (Fig. 5). One can see that the two pentagons after the first approach are building up ten bonds to the Ti atom. By a further approach the bonds between the boron atoms of each of the two pentagons break up. As soon as the unbound pentagons come closer to each other, new bonds between them arise, forming a gym-wheel-like structure. Finally the both pentagons fuse together forming the planar molecular wheel. The 3D to 2D transition makes sure that the most stable structure of the TiB_{10} isomers is the molecular wheel. This transition can be related to a favor overlap between the in-plan *d*-orbitals of Ti atom and the σ-orbitals of boron atoms. Thus, the calculated E_b values of the 2D TiB_n(Opt) clusters (for $n = 1$–10) are presented in (Fig. 6) as a function of the number of boron atoms. One can ascertain that the E_b function, assigned by maroon circles, rises with increasing the number of boron atoms arriving a maximum at 4.86 eV/atom for $n = 10$.

3.3. Boron–nitrogen-doped wheel TiB_nN_{10-n}

As in the previous paper [33], and after the confirmation of the high stability of the molecular wheel TiB_{10}, we doped the titanium boron molecular wheel with nitrogen atoms exactly by replacing boron by nitrogen one by one. The optimization procedure of the molecular wheel was carried out at the BP86/6-31G* level and was done by each new nitrogen atom. It is clear that the system TiB_nN_{10-n} by $n = 10$ becomes TiB_{10}. The first step of nitrogen doping can be started by substitution the TiB_nN_{10-n} system for $n = 9$ getting TiB_9N_1. For $n = 8$, the doped system becomes TiB_8N_2, for $n = 7$ it

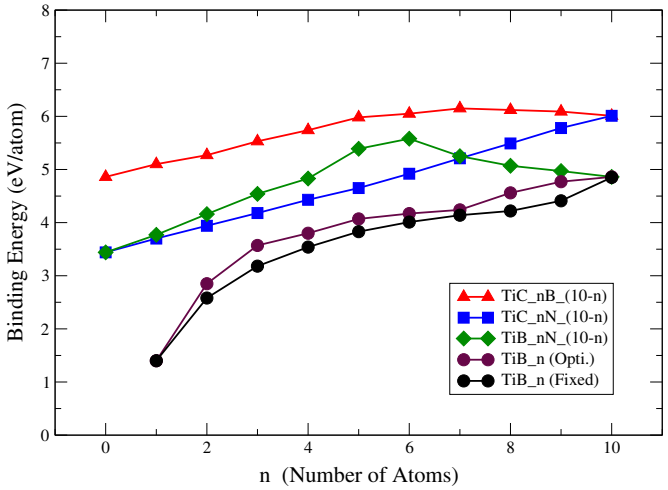

Fig. 6. The stability of molecular wheels $TiB_xC_yN_z$, determined at the BP86/6-31G*.

becomes TiB_7N_3, and finally leads to TiN_{10} for $n = 0$. The substitution of nitrogen atoms occurs first alternately in clockwise direction until $n = 5$ obtaining rotationally symmetrical wheel TiB_5N_5, afterward the residual boron atoms are replaced by nitrogen one by one.

The corresponding E_b values of the TiB_nN_{10-n} system are listed in Table 2 and presented in (Fig. 6), as a function of the number of boron atoms. The bondlengths between Ti, B and N atoms, listed in Table 3, show that these distances are varying between 2.07 and 2.50 Å for Ti–B, and between 2.13 and 2.35 Å for Ti–N. Starting at the E_b value 4.86 eV/atom for TiB_{10} (Fig. 6), which corresponds to $n = 10$ in the TiB_nN_{10-n} system, the E_b values are increasing until $n = 6$ and arriving a maximum of 5.58 eV/atom, then these values decrease with decreasing n approaching to 3.44 eV/atom for TiN_{10} when $n = 0$. The E_b function of the TiB_nN_{10-n} system is assigned by a green diamond.

Further calculations at the high quality basis set cc-pVTZ and the exchange-correlation functionals BP86 and B3LYP were carried out for the TiB_nN_{10-n} system to verify the stability obtained at BP86/6-31G* level of theory. The optimization procedure of this system was done exactly as by the optimization above at BP86/6-31G* level of theory. The resulting E_b of this system is presented in (Fig. 7) as a

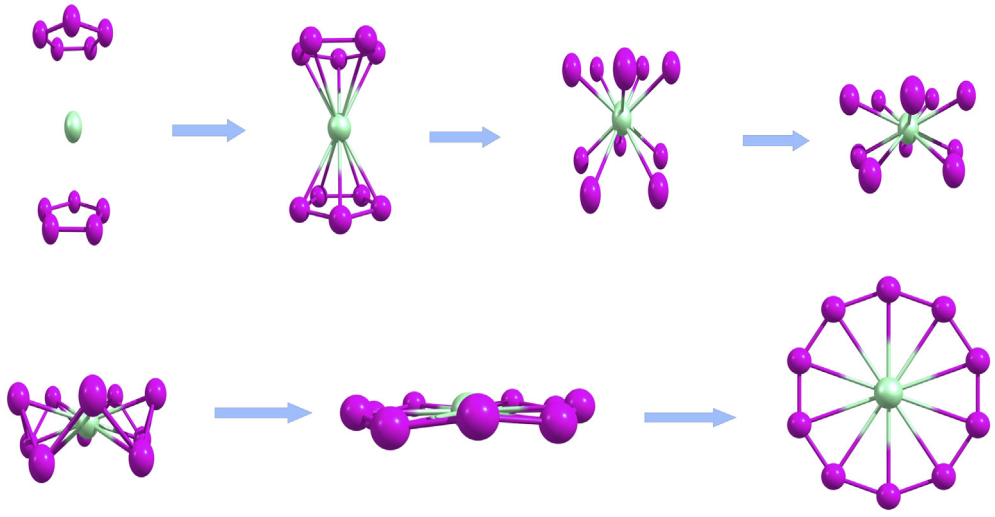

Fig. 5. Structural transition of 3D TiB_{10} cluster into 2D molecular wheel.

Table 2
Binding energy E_b (eV/atom) of molecular wheels, determined at the BP86/6-31G*.

n	TiB_nN_{10-n}	E_b	TiC_nN_{10-n}	E_b	TiC_nB_{10-n}	E_b
10	TiB_{10}	4.86	TiC_{10}	6.01	TiC_{10}	6.01
9	TiB_9N_1	4.97	TiC_9N_1	5.78	TiC_9B_1	6.09
8	TiB_6N_2	5.07	TiC_8N_2	5.49	TiC_8B_2	6.12
7	TiB_7N_3	5.25	TiC_7N_3	5.21	TiC_7B_3	6.15
6	TiB_6N_4	5.58	TiC_6N_4	4.92	TiC_6B_4	6.05
5	TiB_5N_5	5.39	TiC_5N_5	4.65	TiC_5B_5	5.98
4	TiB_4N_6	4.83	TiC_4N_6	4.43	TiC_4B_6	5.74
3	TiB_3N_7	4.54	TiC_3N_7	4.18	TiC_3B_7	5.53
2	TiB_2N_8	4.16	TiC_2N_8	3.94	TiC_2B_8	5.27
1	TiB_1N_9	3.77	TiC_1N_9	3.70	TiC_1B_9	5.10
0	TiN_{10}	3.44	TiN_{10}	3.44	TiB_{10}	4.86

function of the number of the boron atoms. The two E_b functions, calculated at the cc-pVTZ and assigned by TiB_nN_{10-n}/BP86 and TiB_nN_{10-n}/B3LYP, show the same behavior and are quite parallel. Also both E_b functions, obtained at the BP86/cc-pVTZ and B3LYP/cc-pVTZ levels, are respectively assigned by red and blue diamonds and are shifted by around 0.4 eV/atom. Both functions increase with increasing n and arrive maxima at $n = 5$, then they continue to decrease until reaching to their minima at $n = 9$, then increase again for $n = 10$.

3.4. Carbon–nitrogen-doped wheel TiC_nN_{10-n}

We start doping the TiN_{10} system by replacing nitrogen with carbon atoms one by one forming the TiC_nN_{10-n} system. For $n = 1$, it results in the wheel TiC_1N_9, and for $n = 2$ we get TiC_2N_8. We continue to increase n until obtaining the system TiC_{10} for $n = 10$. The substitution of carbon atoms occurs first alternately in clockwise direction until $n = 5$ obtaining the rotationally symmetrical wheel TiC_5N_5, afterward the residual nitrogen atoms are replaced by carbon one by one. The optimization procedure of the molecular wheel was carried out at the BP86/6-31G* level for each substitution of nitrogen with carbon atom. The calculated values E_b of the TiC_nN_{10-n} system are also listed in Table 2 and presented in (Fig. 6) as a function of the number of carbon atoms. The corresponding E_b function, starting from the point 3.44 eV/atom of the TiN_{10} system, increases monotonically up to its maximum of 6.01 eV/atom for the TiC_{10} system by $n = 10$. In (Fig. 6) the E_b function of the TiC_nN_{10-n} system is assigned by a blue square.

As by the previous TiB_nN_{10-n} system, further calculations at the high quality basis set cc-pVTZ as well as at the exchange-correlation functionals BP86 and B3LYP were carried out for the TiC_nN_{10-n} system. The optimization procedure of this system was done exactly as mentioned in the previous paragraph. The resulting E_b of this system is presented in (Fig. 7) as a function of the number of the nitrogen atoms. Both E_b functions, calculated at the cc-pVTZ

Table 3
Bondlengths (Å) of the TiB_nN_{10-n} molecular wheels, determined at the BP86/6-31G*.

n	TiB_nN_{10-n}	R (Ti–B)	R (Ti–N)
10	TiB_{10}	2.50	–
9	TiB_9N_1	2.45	2.17
8	TiB_8N_2	2.42	2.13
7	TiB_7N_3	2.36	2.15
6	TiB_6N_4	tpgoto "2.12	2.33
5	TiB_5N_5	2.08	2.35
4	TiB_4N_6	2.18	2.29
3	TiB_3N_7	2.13	2.27
2	TiB_3N_8	2.13	2.27
1	TiB_1N_9	2.07	2.27
0	TiN_{10}	–	2.28

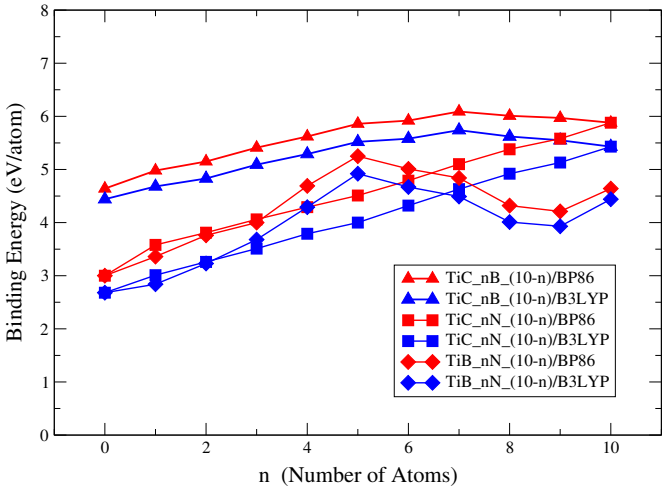

Fig. 7. The stability of molecular wheels $TiB_xC_yN_z$, determined at the BP86/ccpVTZ (red) and B3LYP/cc-pVTZ (blue lower line). (For interpretation of the references to color in this figure legend, the reader is referred to the web version of this article.)

basis set and assigned by TiC_nN_{10-n}/BP86 and TiC_nN_{10-n}/B3LYP, show the same behavior and are quite parallel. Also the both E_b functions, obtained at the BP86/cc-pVTZ and B3LYP/cc-pVTZ levels, assigned respectively by red and blue squares, are shifted also by around 0.4 eV/atom. The latter functions increase monotonically with increasing n and reaches its maxima at $n = 10$.

3.5. Carbon–boron-doped wheel TiC_nB_{10-n}

We continue in the same manner to substitute the carbon atoms in the TiC_{10} system with boron to form the system TiC_nB_{10-n}. It is obvious that by $n = 10$ we have the TiC_{10} system. The insertion of $n = 9$ in the system TiC_nB_{10-n} means, we replace the first carbon atom with boron and receive the system TiC_9B_1. Further insertion of $n = 8$ results in the system TiC_8B_2, for $n = 5$ to get TiC_5B_5 and further down to $n = 0$ getting the final (initial) system TiB_{10}, which is indeed the starting system prior doping. The substitution of carbon with boron atoms up to $n = 5$ occurs first alternately in clockwise direction receiving the rotationally symmetrical wheel system TiC_5B_5. Afterward the residual carbon atoms are replaced by boron atoms approaching the TiB_n system once again. The optimization procedure of the molecular wheel was carried out at the BP86/6-31G* level for each substitution of carbon with boron atom. The calculated E_b values of the TiC_nB_{10-n} system are listed in Table 2 and presented in (Fig. 6) as a function of the number of carbon atoms. The related E_b function in (Fig. 6) starts by the value 6.01 eV/atom for the TiC_{10} system and increases slightly with increasing the number of boron atoms. It approaches its maximum at 6.19 eV/atom by $n = 7$ leading to the system TiC_7B_3. Thereafter it drops towards the E_b value of 4.86 eV/atom of the wheel TiB_{10}. The E_b function of the TiC_nB_{10-n} system is assigned by a red triangle up.

In order to complete the computations of the doped TiC_nB_{10-n} system, additional calculations at high quality basis set cc-pVTZ and at the exchange-correlation functionals BP86 and B3LYP were carried out using the same procedure carried out at BP86/6-31G* level of theory. The resulting E_b values of this system are listed in Table 4 and presented also in (Fig. 7) as a function of the number of the carbon atoms. Both E_b functions, calculated at the cc-pVTZ and BP86 and B3LYP functionals, assigned by TiC_nB_{10-n}/BP86 and TiC_nB_{10-n}/B3LYP, respectively, exhibit analogous behavior and are quite parallel. Also both E_b functions, obtained at the BP86/cc-pVTZ and B3LYP/cc-pVTZ levels, assigned respectively by red and blue

triangles up, are shifted also by around 0.4 eV/atom. Starting by the E_b values of TiC_{10}, both functions increase slightly approaching a maximum at $n = 7$, confirming that the TiC_7B_3 structure is the most stable cluster. Afterward the functions decrease down to $n = 0$ back to the same E_b value of TiB_{10}.

After approaching the energetically favored molecular wheel TiC_7B_3 with 6.19 eV/atom exhibiting the highest stability, we proceed further to present some geometric and electronic properties obtained at the BP86/6-31G* level of theory. The wheel structure of TiC_7B_3 is illustrated in (Fig. 8) with the corresponding ground state C_{2v} ($^2A_1$). The related bondlengths Ti–B and Ti–C are respectively 2.33 and 2.18 Å in average, and the bondlength B–C is about 1.4 Å. The highest four occupied molecular orbitals (MOs) of α-spins 37, 38, 39, and 40, are characterized by σ-, and π-bonds and are also presented in (Fig. 8). The coefficients of the HOMO 40 are dominated by the Ti($3d_{yz}$), B($2p_y$), and C($3s,2p_y,2p_z$) atomic orbitals showing σ-bonds. Thus the MO 40 of TiC_7B_3 shows clearly that the *d*-orbital of the Ti atom participates actively in the bonding and the in-plane d_{yz} orbital is interacting radially with the p_y and p_z orbitals of boron and carbon atoms. The HOMO–LUMO gaps of α- and β-spins are 0.052 and 0.088 Hartree, respectively.

The Mulliken analysis of the electron charge transfer in the molecular wheel TiC_7B_3 occurs slightly from titanium to boron and carbon atoms. The extent of electron charge of titanium is 0.277, while the average of the charge transfer to the seven carbon atoms is likely −0.023e and to the three boron atoms is likely −0.044e. In order to determine the aromaticity of the TiC_7B_3 wheel, we have calculated the NICS values to be −73.64 ppm at 1.0 Å and −25.14 ppm at 2.0 Å above the central atom Ti. The calculated eigenvalues of the Hessian matrix are all real thus the frequencies are positive. The smallest and largest frequency modes are respectively 62 and 1809 cm^{-1}, with the highest infrared intensity at 1635 cm^{-1}. These modes indicate that the structure of the TiC_7B_3 molecular wheel corresponds to a global minimum at the potential energy surface. The reasons behind this stability can be related to the sp^2-hybridization, the overlap of in-plane *d*-orbitals of metal atom with the σ-orbitals of boron and carbon atoms, as well as the overlap of d_z^2-orbitals of metal atom with the π-orbitals of boron and carbon atoms, which indicates the aromaticity of the wheel.

3.6. The MC_nB_{10-n} systems (for M = Sc to Zn and n = 5–8)

In the previous section we have found that the most stable molecular wheels are those composed of different weights of carbon and boron atoms beside a titanium atom as the center. The most stable one is TiC_7B_3 followed by TiC_8B_2, TiC_6B_4 and TiC_5B_5 wheels. In order to find out whether the transition metal atom Ti at the center has the best chemical bonds to the surrounding atoms, we have recalculated these MC_nB_{10-n} wheels (for $n = 5–8$) at BP86/6-31G* and B3P86/cc-pVTZ levels, considering for M the transition metal atoms of the first row Sc, Ti, V, Cr, Mn, Fe, Co, Ni, Cu, and Zn. The E_b of the wheels TiC_7B_3, TiC_6B_4 and TiC_5B_5, calculated at the BP86/6-31G* level, are listed in Table 5 and plotted in (Fig. 9), as a function of the transition metal atoms. These functions have similar behavior showing the highest value for Ti then decrease downward to the smallest value for Zn. The E_b of the wheels TiC_8B_2, TiC_7B_3 and TiC_6B_4, calculated at the B3P86/cc-pVTZ level of theory, are listed in Table 6 and plotted in (Fig. 10), as a function of the transition metal atoms. These functions have also similar behavior showing again the highest values for Sc, Ti, and V, which are larger than 6 eV/atom. The E_b function of TiC_6B_4 decreases nearly monotonically downward Zn, while the E_b functions of both TiC_8B_2 and TiC_7B_3 are moving over two turning points afterward down to the smallest value for Zn. It is important to mention here that different spin multiplicities of these systems were computed by the BP86/6-31G* and B3P86/cc-pVTZ calculations above, and the spin multiplicity of the lowest ground state energy is considered and listed also in Tables 5 and 6 and given in parenthesis as (Mult.) by neglecting spin-orbit coupling.

Table 4
Binding energy E_b (eV/atom) of molecular wheels, determined at the B3LYP/cc-pVTZ and BP86/cc-pVTZ.

n	TiB_nN_{10-n}	B3LYP	BP86	TiC_nN_{10-n}	B3LYP	BP86	TiC_nB_{10-n}	B3LYP	BP86
10	TiB_{10}	4.43	4.64	TiC_{10}	5.43	5.88	TiC_{10}	5.43	5.88
9	TiB_9N_1	3.93	3.35	TiC_9N_1	5.13	5.57	TiC_9B_1	5.55	5.97
8	TiB_6N_2	4.01	4.33	TiC_8N_2	4.93	5.38	TiC_8B_2	5.62	6.02
7	TiB_7N_3	4.49	4.84	TiC_7N_3	4.63	5.10	TiC_7B_3	5.74	6.09
6	TiB_6N_4	4.67	5.01	TiC_6N_4	5.21	4.79	TiC_6B_4	5.58	5.92
5	TiB_5N_5	4.91	5.25	TiC_5N_5	4.00	4.52	TiC_5B_5	5.52	5.86
4	TiB_4N_6	4.29	4.69	TiC_4N_6	3.79	4.29	TiC_4B_6	5.29	5.62
3	TiB_3N_7	3.68	4.00	TiC_3N_7	3.51	4.06	TiC_3B_7	5.09	5.41
2	TiB_2N_8	3.23	3.76	TiC_2N_8	3.26	3.81	TiC_2B_8	4.83	5.15
1	TiB_1N_9	2.84	3.36	TiC_1N_9	3.01	3.58	TiC_1B_9	4.68	4.98
0	TiN_{10}	2.38	3.00	TiN_{10}	3.38	3.00	TiB_{10}	4.43	4.64

4. Summary and conclusions

The current follow-up study shows that including exchange-correlation functionals and using high quality basis sets reproduce more accurate and reliable results. In addition, the calculations at high level of theory, change the sequence of stability and predict new composition of transition metal, boron, carbon and

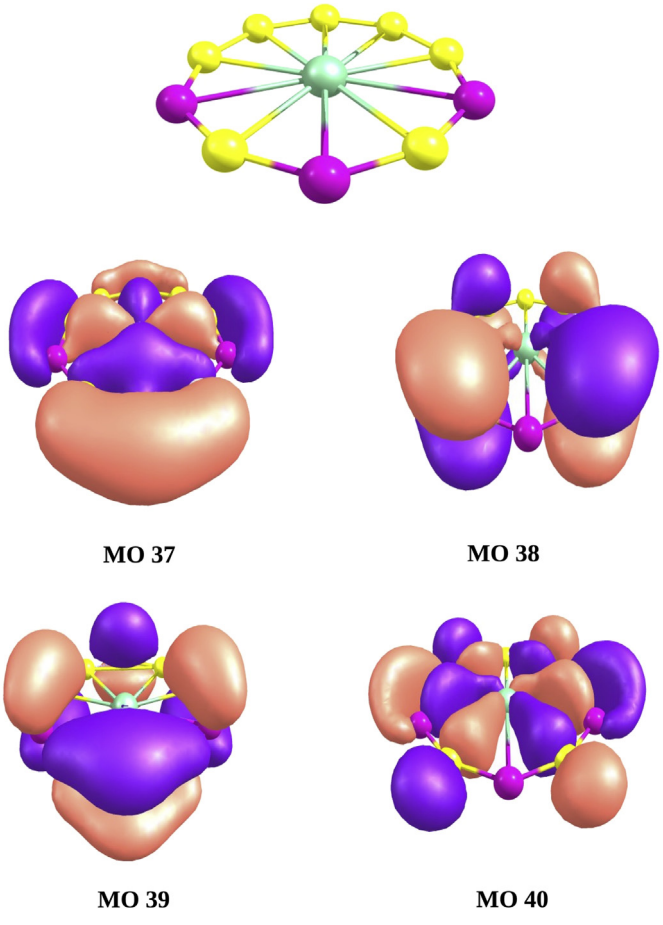

Fig. 8. The most stable molecular wheel TiB_3C_7 and four HOMOs of α-spins.

Table 5
Binding energy E_b (eV/atom) and spin-multiplicity of MB_5C_5, MB_4C_6 and MB_3C_7, determined at the BP86/6-31G*.

M-Atom	MB_5C_5 (Mult.)	MB_4C_6 (Mult.)	MB_3C_7 (Mult.)
Sc	5.87 (3)	6.01 (2)	6.11 (3)
Ti	5.98 (4)	6.13 (3)	6.19 (2)
V	5.95 (5)	6.10 (2)	6.13 (3)
Cr	5.96 (2)	6.11 (3)	6.10 (2)
Mn	5.89 (1)	6.05 (4)	5.98 (3)
Fe	5.75 (4)	5.90 (3)	5.96 (4)
Co	5.72 (3)	5.86 (4)	5.87 (1)
Ni	6.00 (4)	6.14 (1)	6.07 (4)
Cu	5.95 (1)	6.08 (2)	6.00 (3)
Zn	5.30 (4)	5.46 (3)	5.68 (4)

Table 6
Binding energy E_b (eV/atom) and spin-multiplicity of MB_4C_6, MB_3C_7 and MB_2C_8, determined at the B3P86/cc-pVTZ.

M-Atom	MB_4C_6 (Mult.)	MB_3C_7 (Mult.)	MB_2C_8 (Mult.)
Sc	5.91 (2)	6.01 (3)	6.12 (2)
Ti	5.98 (3)	6.07 (2)	6.14 (1)
V	5.87 (2)	6.10 (3)	6.11 (4)
Cr	5.66 (3)	6.00 (2)	6.03 (3)
Mn	5.64 (4)	5.83 (3)	5.85 (4)
Fe	5.66 (3)	5.88 (4)	5.79 (3)
Co	5.57 (4)	5.85 (1)	5.89 (4)
Ni	5.54 (1)	5.89 (4)	5.93 (1)
Cu	5.38 (2)	5.76 (3)	5.80 (2)
Zn	5.19 (3)	5.43 (4)	5.56 (1)

nitrogen atoms. The first remarkable results is that some of the 2D and 3D TiB_n clusters of planar fan-like and 3D pyramidal optimized structures, respectively, have very close binding energy per atom, obtained at the BP86/6-31G* level as shown in Table 1. The E_b value 4.07 eV/atom of the 2D-TiB_5 is only 0.02 eV higher than that of the 3D-TiB_5 pyramidal structure, and the E_b value 4.77 of the 2D-TiB_9 is with 0.03 eV rather slightly higher than that of the 3D-TiB_9 pyramid. Therefore one can consider the energies of the 2D and 3D structures of TiB_5 and of TiB_9 as degenerate.

On the other hand, the E_b value 4.50 eV/atom of the 3D-TiB_7 is with 0.23 eV higher than that of the 2D-TiB_7 planar structure, while the E_b value 4.86 eV/atom of the 2D-TiB_{10}, 0.25 eV larger than that of 3D-TiB_{10} pyramid. It is also worth to perceive that even clusters except of TiB_{10} are 3D and prefer higher spins, while odd clusters are 2D and prefer lower spins. The negative values of the harmonic vibrational frequencies of some 2D and 3D clusters confirm that their geometrical structures are in transition state, and the global minimum still not found. One can conclude that the competition between 2D and 3D TiB_n clusters (for $n = 3–8$) needs a deeper and detailed analysis and to be carried out in a new study. Furthermore, the TiB_n clusters (for $n = 9$ and 10) prefer to be planar wheels and that spin states play a basic role. However, the TiC_x (for $x = 2–5$) clusters, determined by photoelectron spectroscopy [32], have also planar cyclic structures, similar to those of the 2D TiB_n clusters.

The development of the 3D TiB_n pyramidal structures into the 2D molecular wheels can be described as follows: the heights of these pyramids, in which Ti is always as an apex atom, are reduced successively with increasing the number of boron atoms until $n = 8$ having nearly a flat octagonal pyramid, then for $n = 9$ the height is vanished and the pyramid transforms into a wheel. The next conclusion is that the Ti atom can accommodate only 10 boron atoms around, and thus having the highest coordination number.

In order to verify whether the molecular wheel of TiB_{10} is truly stable structure, we have considered and studied different 3D isomers adopted from common structures known in the (in)organic chemistry. They were optimized at the BP86/6-31G* level of theory in view of some symmetry constraints. The calculations have shown that the 2D molecular wheel is energetically much more favored than all 3D isomers of TiB_{10}. One of these isomers, the TiB_{10}-D_{5d}, is composed of two staggered pentagons localized above and below the Ti atom. This isomer seems to prefer a structural transition from 3D into 2D seeking an energy minimum. The both staggered pentagons approach to each other and fused together forming the planar molecular wheel resulting the lowest energy of all TiB_{10} isomers. Hereafter, we conclude that the 2D molecular wheel of TiB_{10} is energetically favored over all other 3D structures and thus obtaining an E_b value of 4.86 eV/atom and being the most stable structure between all TiB_{10} isomers.

After the assurance that the molecular wheel TiB_{10}, composed of Ti and boron atoms only, is most stable structure, arises the question whether doping with other light atoms would improve the stability. Therefore, we substitute first boron with nitrogen forming the TiB_nN_{10-n} system. The calculations have shown that the stability increases and reaches to its maximum 5.58 eV/atom at $n = 6$, leading to the most stable TiB_6N_4 wheel at the BP86/6-31G* level. Nevertheless, the stability of the TiB_5N_5 wheel at the B3LYP/cc-pVTZ and BP86/cc-pVTZ level of theory arrives a maximum first by $n = 5$ and the corresponding binding energy E_b reduces to 4.91

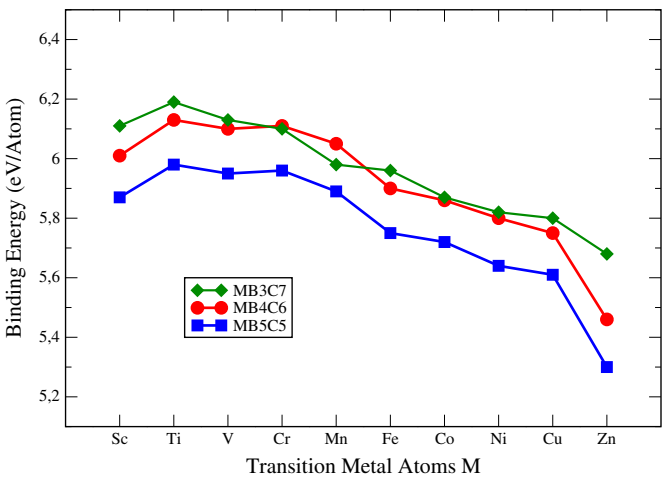

Fig. 9. The stability of molecular wheels $MB_xC_yN_z$, determined at the BP86/6-31G*.

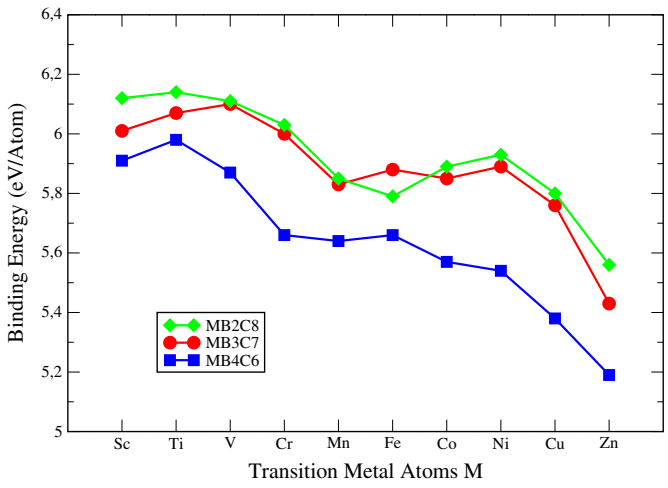

Fig. 10. The stability of molecular wheels $MB_xC_yN_z$, determined at the B3P86/ccpVTZ.

and 5.25 eV/atom, respectively. However, the functions of E_b, calculated at these levels of theory, drop down approaching their minima by $n = 10$.

We have already seen that substitution of nitrogen by boron atoms in the TiN_nB_{10-n} system leads for $n = 10$ to the TiN_n wheel with the E_b of 3.44 eV/atom at BP86/6-31G* level. Following the same procedure we doped this TiN_n wheel with carbon obtaining the TiC_nN_{10-n} system. The calculations have shown that substitution of nitrogen by carbon improves essentially the stability. The E_b functions of $TiC_{10}N_{10-n}$, determined at the BP86/6-31G*, B3LYP/cc-pVTZ and BP86/cc-pVTZ level of theory, increase monotonically with increasing the number of carbon atoms arriving by $n = 10$ a maximum of 6.01, 5.43 and 5.88 eV/atom, respectively. Finally, we continue replacing carbon by boron so that the E_b function of the TiC_nB_{10-n} system sustains a slight improvement in stability but only by a substitution of four boron atoms. Afterward the E_b function decreases until arriving the value of the starting point TiB_{10}. Thus, the TiC_7B_3 wheel, with an E_b value of 6.19 eV/atom, Table 5, is elected to be the most stable wheel, followed by TiC_8B_2 and TiC_6B_4.

All wheel systems studied above were computed with the Ti atom at the center. In order to verify whether there is another element of the first row of transition metals which could exhibit better stability than with Ti, we have established further computations for the systems MC_7B_3, MC_8B_2, MC_6B_4 and MC_5B_5 for M = Sc to Zn. The corresponding E_b functions of these systems, calculated at the BP86/6-31G* and B3P86/cc-pVTZ level of theory, have maxima by the metal atom Ti. Herewith we proved that the combination MC_7B_3 is energetically the most favored molecular wheel. It is to perceive that the E_b functions at the BP86/6-31G* level have a maximum by Ti, they decrease downward the smallest value for Zn. Different behavior is found for the E_b functions at the B3P86/cc-pVTZ level of theory. The E_b function of MC_6B_4 increases slightly at Ti, then it decreases downwards to Zn with a buckle by Fe. The E_b functions of MC_7B_3 and MC_8B_2 have similar behavior, so that they respectively increase slightly to maxima by V and Ti, then they move over to two turning points downwards to Zn. The calculations of the MC_nB_{10-n} systems (for M = Sc to Zn and $n = 5–8$) at the BP86/6-31G* and B3P86/cc-pVTZ level of theory were carried out for different spin multiplicities. The spin multiplicity of the lowest ground state energy was considered to determine the stability.

Finally, we conclude that we have developed a new path of molecular wheels and determined how to obtain a wheel starting by TiB adding boron atoms until filling the space around Ti atom accommodating maximal 10 boron atoms. The structures of 2D and 3D TiB_n (for $n = 3–8$) clusters are in competition, but nevertheless those of the TiB_n (for $n = 9–10$) clusters prefer to be 2D molecular wheels. The stability of the TiB_{10} wheel can be enhanced by substituting boron by nitrogen or carbon. The calculations, obtained at the BP86/6-31G* level of theory, have shown that the TiC_7B_3 has the highest stability of 6.19 eV/atom with the ground state C_{2v} ($^2A_1$). The corresponding molecular orbitals HOMOs are characterized with σ-bonds and π-bonds, as expected. The MOs of the TiC_7B_3 wheel show clearly that the *d*-orbitals of Ti atom participate actively in the bonding and those in-plane and out-of-plane orbitals are interacting with π and σ orbitals of boron and carbon atoms. We have also calculated MC_7B_3 for M = Sc to Zn and found that the most stable molecular wheel favors Sc, Ti, and V at the center, with values larger than 6 eV/atom. However, there are still some open questions like the sequence or positions of boron and carbon atoms around the center Ti and whether the small atoms prefer different combinations. Also the competition between the 2D and 3D TiB_n clusters for ($n = 3–7$) needs to be verified by more accurate methods. Could hydrogen or alkali-metals influence the stability and properties of molecular wheels invoking the Jahn–Teller–Effect particularly by rotationally symmetrical wheels with highest occupied degenerated molecular orbitals. These issues will be the subjects of our next investigation.

References

[1] I. Boustani, in: Michael Springborg (Ed.), Chemical Modelling: Applications and Theory, vol. 8, Royal Society of Chemistry, 2011, pp. 1–44.
[2] A.R. Oganov, J.-H. Chen, C. Gatti, Y.-Z. Ma, Y.-M. Ma, C.W. Glass, Z.-X. Liu, T. Yu, O.O. Kurakevych, V.L. Solozhenko, Nature 457 (2009) 863.
[3] L. Hanley, S.L. Anderson, J. Chem. Phys. 89 (1988) 2848.
[4] L. Hanley, J. Whitten, S.L. Anderson, J. Phys. Chem. 92 (1988) 5803.
[5] R. Kawai, J.H. Weare, J. Chem. Phys. 95 (1991) 1151.
[6] H. Kato, E. Tanaka, J. Comput. Chem. 12 (1991) 1097.
[7] H. Kato, K. Yamashita, K. Morokuma, Chem. Phys. Lett. 190 (1992) 361.
[8] I. Boustani, Chem. Phys. Lett. 240 (1995) 135.
[9] I. Boustani, Phys. Rev. B 55 (1997) 16426.
[10] I. Boustani, A. Quandt, P. Kramer, Europhys. Lett. 36 (1996) 583.
[11] I. Boustani, A. Quandt, Europhys. Lett. 39 (1997) 527.
[12] I. Boustani, A. Quandt, E. Fernandez, A. Rubio, J. Chem. Phys. 110 (1999) 3176.
[13] I. Boustani, J. Solid State Chem. 133 (1997) 182.
[14] K.C. Lau, R. Pandey, J. Phys. Chem. B 112 (2008) 10217.
[15] C. Özdoğan, S. Mukhopadhyay, W. Hayami, Z.B. Güvenç, R. Pandey, I. Boustani, J. Phys. Chem. C 114 (2010) 4362.
[16] I. Boustani, Y. Li, V. Bonačić-Koutecký, J. Koutecký, 1990, unpublished results.
[17] P. Bonačić-Koutecký, Fantucci, J. Koutecký, Chem. Rev. 91 (1991) 1053.
[18] I. Boustani, Int. J. Quantum Chem. 52 (1994) 1081.
[19] H.-J. Zhai, A.N. Alexandrova, K.A. Birch, A.I. Boldyrev, L.-S. Wang, Angew. Chem. Int. Ed. 43 (2003) 2004–2008.
[20] (a) J. Chandrasekhar, E.D. Jemmis, P. v. R. Schleyer, Tetrahedron Lett. 20 (1979) 3707;
(b) A.B. McEven, P. v. R. Schleyer, J. Org. Chem. 51 (1986) 4357;
(c) P. v. R. Schleyer, H. Jiao, M.N. Glukhovtsev, J. Chandrasekhar, E. Kraka, J. Am. Chem. Soc. 116 (1994) 10129;
(d) A.A. Fonkin, H. Jiao, P. v. R. Schleyer, J. Am. Chem. Soc. 120 (1998) 9364.
[21] P.W. Fowler, B.R. Gray, Inorg. Chem. 46 (2007) 2892.
[22] T.B. Tai, R.W.A. Havenith, J.L. Teunissen, A.R. Dok, S.D. Hallaert, M.T. Nguyen, A. Ceulemans, Inorg. Chem. 52 (2013) 10595.
[23] P. v. R. Schleyer, C. Maerker, A. Dransfeld, H. Jiao, N.J. R. v. E. Hommes, J. Am. Chem. Soc. 118 (1996) 6371.
[24] C. Romanescu, T.R. Galeev, W.-L. Li, A.I. Boldyrev, L.-S. Wang, Angew. Chem. 123 (2011) 9506.
[25] W.-L. Li, C. Romanescu, Z.A. Piazza, L.-S. Wang, Phys. Chem. Chem. Phys. 14 (2012) 13663.
[26] T. Heine, G. Merino, Angew. Chem. Int. Ed. 51 (2012) 4275–4276.
[27] I. Gutman, M. Milun, N.J. Trinajistic, J. Am. Chem. Soc. 99 (1977) 1692.
[28] J.-i. Aihara, J. Am. Chem. Soc. 98 (1975) 2750.
[29] Y. Nakagami, N.-Y. Suzuki, R. Sekine, T. Matsuura, J.-i. Aihara, Bull. Chem. Soc. Jpn. 4 (2012) 475–480.
[30] Y.-L. Liao, C.L. Cruz, P. v. R. Schleyer, Z.-F. Chen, Phys. Chem. Chem. Phys. 14 (2012) 14898.
[31] (a) T.R. Galeev, C. Romanescu, W.-L. Li, L.-S. Wang, A.I. Boldyrev, Angew. Chem. 124 (2012) 2143;
(b) Angew. Chem. Int. Ed. 51 (2012) 2101.
[32] X.-B. Wang, C.-F. Ding, L.-S. Wang, J. Phys. Chem. A 101 (1997) 7699.
[33] I. Boustani, R. Pandey, Solid State Sci. 14 (2012) 1591.
[34] A.D. Becke, Phys. Rev. A 38 (1988) 3098.
[35] J.P. Perdew, Phys. Rev. B 33 (1986) 8822.
[36] A.D. Becke, J. Chem. Phys. 98 (1993) 5648.
[37] C. Lee, W. Yang, R.G. Parr, Phys. Rev. B 37 (1988) 785.
[38] GAMESS-UK is a package of ab initio programs. See: http://www.cfs.dl.ac.uk/gamess-uk/index.shtml; M.F. Guest, I.J. Bush, H.J.J. van Dam, P. Sherwood, J.M.H. Thomas, J.H. van Lenthe, R.W.A. Havenith, J. Kendrick, The GAMESS-UK electronic structure package: algorithms, developments and applications, Mol. Phys. 103 (2005) 719–747.
[39] M. Valiev, E.J. Bylaska, N. Govind, K. Kowalski, T.P. Straatsma, H.J.J. van Dam, D. Wang, J. Nieplocha, E. Apra, T.L. Windus, W.A. de Jong, NWChem: a comprehensive and scalable open-source solution for large scale molecular simulations, Comput. Phys. Commun. 181 (2010) 1477.
[40] (a) Frank Neese, The ORCA program system, WIREs Comput. Mol. Sci. 2 (2012) 73–78;
(b) R. Izsak, F. Neese, An overlap fitted chain of spheres exchange method, J. Chem. Phys. 135 (2011) 144105;
(c) S. Kossmann, F. Neese, Efficient structure optimization with second order many body perturbation theory: the RIJCOSX-MP2 method, J. Chem. Theory Comput. 6 (2010) 2325–2338;
(d) S. Kossmann, F. Neese, Comparison of two efficient approximate Hartree–Fock approaches, Chem. Phys. Lett. 481 (2009) 240–243;
(e) F. Neese, F. Wennmohs, A. Hansen, U. Becker, Efficient, approximate and parallel Hartree–Fock and hybrid DFT calculations. A chain-of-spheres algorithm for the Hartree–Fock exchange, Chem. Phys. 356 (2009) 98–109;
(f) F. Neese, An improvement of the resolution of the identity approximation for the calculation of the coulomb matrix, J. Comput. Chem. 24 (2003) 1740–1747.

[41] M.J. Frisch, G.W. Trucks, H.B. Schlegel, G.E. Scuseria, M.A. Robb, J.R. Cheeseman, J.A. Montgomery Jr., T. Vreven, K.N. Kudin, J.C. Burant, J.M. Millam, S.S. Iyengar, J. Tomasi, V. Barone, B. Mennucci, M. Cossi, G. Scalmani, N. Rega, G.A. Petersson, H. Nakatsuji, M. Hada, M. Ehara, K. Toyota, R. Fukuda, J. Hasegawa, M. Ishida, T. Nakajima, Y. Honda, O. Kitao, H. Nakai, M. Klene, X. Li, J.E. Knox, H.P. Hratchian, J.B. Cross, C. Adamo, J. Jaramillo, R. Gomperts, R.E. Stratmann, O. Yazyev, A.J. Austin, R. Cammi, C. Pomelli, J.W. Ochterski, P.Y. Ayala, K. Morokuma, G.A. Voth, P. Salvador, J.J. Dannenberg, V.G. Zakrzewski, S. Dapprich, A.D. Daniels, M.C. Strain, O. Farkas, D.K. Malick, A.D. Rabuck, K. Raghavachari, J.B. Foresman, J.V. Ortiz, Q. Cui, A.G. Baboul, S. Clifford, J. Cioslowski, B.B. Stefanov, G. Liu, A. Liashenko, P. Piskorz, I. Komaromi, R.L. Martin, D.J. Fox, T. Keith, M.A. Al-Laham, C.Y. Peng, A. Nanayakkara, M. Challacombe, P.M.W. Gill, B. Johnson, W. Chen, M.W. Wong, C. Gonzalez, J.A. Pople, Gaussian 03, Revision C.02, Gaussian, Inc., Wallingford CT, 2004.